

Diamagnetic nature of stratified thin metals in visible range

Masanobu Iwanaga*

Department of Physics, Graduate School of Science, Tohoku University, Sendai 980-8578, Japan

(Dated: July 25, 2018)

It is numerically demonstrated that effectively strong diamagnetic resonance emerges at visible frequencies in stratified metal-dielectric metamaterials. The effective optical constants are extracted by two-complex reflectivity method. It is clarified that the effective diamagnetic response originates from local diamagnetism at stratified thin metals. The effective diamagnetism is crucially sensitive to the structure of unitcell. The effective diamagnetic response is always associated with effective plasma frequency and is therefore regarded as a magnetic component of the collective excitation.

PACS numbers: 42.25.Bs, 42.70.Qs, 78.20.Ci, 73.22.Lp

I. INTRODUCTION

Photonic metamaterials are trials to invent and produce novel electromagnetic (EM) states by modifying periodic structures in which constituents have the same optical constants with the bulk materials. The trials started at gigahertz, and has proceeded to terahertz and optical frequencies. The rapid progress was reviewed in [1, 2]. The strategy is significantly different from nano-scale materials science in which quantum size effect on electronic states is a key. In metamaterials, novel effective EM states are explored by controlling the geometrical structures. The effective EM states are solutions of Maxwell equations for a homogenized system obtained by coarse-graining and represent averaged EM fields approximately.

Recent metamaterial optics usually employs a retrieval way to evaluate effective optical constants [3]. The procedure is briefly explained as follows: When one knows complex transmissivity and reflectivity (called S parameters) for a finitely thick object, one can numerically calculate (or retrieves) the effective permittivity and permeability by substituting the S parameters into the transmission and reflection formulas, which hold for a finitely thick material of effective optical constants. The way was first introduced in 2002 [3] and has been called retrieval way.

The retrieval way is algorithmic and not rigorous compared with the effective media description, which has been studied over one century [4, 5, 6] since Maxwell-Garnet [7, 8]. The effective media descriptions are usually derived for specified structures by assuming analytical models and the long wavelength limit. The difference between the effective media description and recent retrieval way was already described in the introduction of [9]. In short, the effective media description is derived analytically for ideally large objects under the long wavelength approximation, whereas the retrieval way transforms the S parameters into effective optical constants in a practical way.

In the retrieval way, there are two distinct points from the effective media description: (i) the interface of metamaterials play a crucial role because the S parameters are sensitive to the surface layers; (ii) the description using effective optical constants turned out to be approximately valid for several artificial metamaterials beyond the long wavelength limit [9]. By use of the retrieval way, effective magnetic responses and negative refraction at optical frequencies have been demonstrated experimentally [10, 11, 12]. Those metamaterials exhibit novel optical states, which are exceptions to the statement that permeability is unity at optical frequencies [13].

A simple theoretical analysis presented a possibility of super-resolution by a thin metal film [14] and the sub-diffraction-limited image was shown experimentally [15]. It is expected that near-EM-field enhancement is induced to compensate the loss at resonance with exploiting thin metallic layers. Another experimental result on transmission was reported which supports the enhancement of EM fields by stratified thin metals [16]. It was also shown that the enhancement is associated with high magnetic field in thin metals [17]. Besides, it was recently argued that negative refractive response appears in stratified stacks composed of metal-dielectric several layers [18, 19]. Thus, the magnetic response in metallic thin films attracts great interest, connecting to novel optical phenomena.

In this paper, stratified metal-dielectric metamaterials (SMDM) are specified to clarify the effective magnetic response at visible frequencies. Typical optical properties of SMDM have been shown in an earlier publication [20]. Here, the effective magnetic response is focused on and explored with modifying the structure of unitcell. Figure 1 shows the schematic drawing of SMDM and the coordinate configuration. The metal is set to be Ag and the dielectric is MgF_2 . The thickness of metal and dielectric are 15 and 60 nm, respectively. The periodicity is then 75 nm. The thickness of Ag layers was set to ensure using dielectric constant of bulk silver in literature [21].

In Sec. II, two-complex reflectivity method (TCRM) are described. Numerical results are shown in Sec. III, and the implication is explored to elucidate the origin of effective magnetic response. More discussion and comparison with other types of magnetism reported so far are given in Sec. IV.

*Electronic address: M.Iwanaga@osa.org

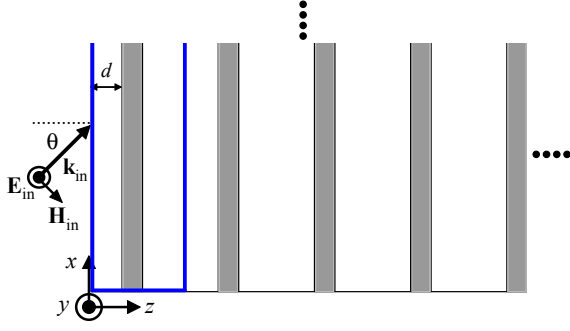


FIG. 1: Schematic drawing for structure of SMDM and coordinate configuration. Gray indicates metal (Ag) and white dielectric (MgF_2). Blue bold line indicates the unitcell of SMDM. Incident light sheds on xy plane with s polarization (*i.e.* $\mathbf{E}_{\text{in}} \parallel y$) and incident angle θ . The thickness of surface layer is denoted by d . In this configuration, the two products of ε_y/μ_x and $\mu_x\mu_z$ are determined from two incident angles. Details are given in Sec. II.

II. TWO-COMPLEX REFLECTIVITY METHOD

In this study, bulk SMDM is analyzed which is thick enough to eliminate transmission, and full components of ε and μ tensors are extracted by TCRM. Although the scheme of TCRM was reported already [20], the full description is provided in the following.

Since the structure of SMDM is uniaxial, effective tensors of permittivity ε and permeability μ are assumed to be diagonal and uniaxial:

$$\varepsilon = \begin{pmatrix} \varepsilon_x & 0 & 0 \\ 0 & \varepsilon_y & 0 \\ 0 & 0 & \varepsilon_z \end{pmatrix}, \quad \mu = \begin{pmatrix} \mu_x & 0 & 0 \\ 0 & \mu_y & 0 \\ 0 & 0 & \mu_z \end{pmatrix}. \quad (1)$$

The optical axis is set to be the z axis, and then the two relations of $\varepsilon_x = \varepsilon_y$ and $\mu_x = \mu_y$ hold in Eq. (1).

In linear and axial media, electric and magnetic flux densities are expressed using permittivity and permeability tensors as

$$\mathbf{D} = \varepsilon_0 \varepsilon \mathbf{E}, \quad (2)$$

$$\mathbf{B} = \mu_0 \mu \mathbf{H}, \quad (3)$$

where ε_0 and μ_0 are permittivity and permeability in vacuum, respectively.

First, the boundary conditions of Maxwell equations are taken into account. In Fig. 1, incident wavenumber vector \mathbf{k}_{in} is in the xz plane and then refracted wave has the wavevector \mathbf{k} in the xz plane. We here introduce normalized refracted wavevector $\hat{\mathbf{k}} = \mathbf{k}/k_0$ where k_0 is wavenumber of light in vacuum, and can write $\hat{\mathbf{k}}$ as

$$\hat{\mathbf{k}} = \begin{pmatrix} \hat{k}_x \\ 0 \\ \hat{k}_z \end{pmatrix}. \quad (4)$$

Then, complex reflectivity r_s under s polarization (that is, $\mathbf{E}_{\text{in}} \parallel y$) in Fig. 1 is easily derived from the Maxwell boundary conditions [22]; the equation for r_s is sometimes called Fresnel formula [23]. After simple modification, the next equation is obtained:

$$\frac{\hat{k}_z(\theta)}{\mu_x} = \frac{n_0 \cos \theta}{\mu_0} \frac{1 - r_s(\theta)}{1 + r_s(\theta)}, \quad (5)$$

where θ is incident angle, and n_0 denotes the refractive index in vacuum. In particular, $\hat{k}_z(0)$ is refractive index along the z axis.

Next, the equation of dispersion is included in TCRM. When the EM fields are monochromatic plane waves and proportional to $\exp(i\mathbf{k} \cdot \mathbf{r} - i\omega t)$, the two of the Maxwell equations are

$$i\mathbf{k} \times \mathbf{E} = i\omega \mathbf{B}, \quad (6)$$

$$i\mathbf{k} \times \mathbf{H} = -i\omega \mathbf{D}. \quad (7)$$

Note that the fields \mathbf{E} , \mathbf{H} , \mathbf{D} , and \mathbf{B} in Eqs. (6) and (7) are independent of (\mathbf{r}, t) .

When the solution of plane wave is assumed, it is generally allowed that the ε and μ tensors depend on the frequency ω and wavevector \mathbf{k} ; that is, the ε and μ tensors have frequency and spatial dispersions ($\varepsilon = \varepsilon(\omega, \mathbf{k})$ and $\mu = \mu(\omega, \mathbf{k})$) [13]. However, it is for the present assumed that the ε and μ tensors are independent of \mathbf{k} . In solid crystals, the μ tensor is set to be unity at optical frequencies and independent of \mathbf{k} , and the spatial dispersion of ε tensor is often so weak that it is frequently negligible [13].

Equations (2) and (7) yield Eq. (8), and Eq. (9) is derived with help of Eqs. (3) and (6):

$$\varepsilon \mathbf{E} = -\frac{1}{\varepsilon_0 \omega} \mathbf{k} \times \mathbf{H} \quad (8)$$

$$= -\frac{1}{\varepsilon_0 \omega} \mathbf{k} \times \left[\frac{1}{\mu_0 \omega} \mu^{-1} (\mathbf{k} \times \mathbf{E}) \right] \quad (9)$$

$$= -\hat{\mathbf{k}} \times \left[\mu^{-1} (\hat{\mathbf{k}} \times \mathbf{E}) \right]. \quad (10)$$

Equation (10) is obtained by using $\mathbf{k} = k_0 \hat{\mathbf{k}}$ and the relation

$$\frac{k_0^2}{\varepsilon_0 \mu_0 \omega^2} = 1.$$

The determinant of coefficient matrix for \mathbf{E} in Eq. (10) has to be zero to have nontrivial solution; therefore, Eq. (10) yields a general constraint between ε and μ for a given $\hat{\mathbf{k}}$. The constraint condition is equation of dispersion and can be regarded as generalization of Fresnel equation. Historically, Fresnel equation was derived under the condition of $\mu = 1$, gave the equation concerning ε for a given $\hat{\mathbf{k}}$, and has been usually employed to explain optical phenomena, *e.g.* birefringence, in solid crystals [13].

Under s polarization, Eq. (10) is modified using Eq. (1) and (4) :

$$\begin{aligned} \varepsilon \begin{pmatrix} 0 \\ E_y \\ 0 \end{pmatrix} &= -\hat{\mathbf{k}} \times \left[\mu^{-1} \begin{pmatrix} -\hat{k}_z E_y \\ 0 \\ \hat{k}_x E_y \end{pmatrix} \right] \\ &= \begin{pmatrix} 0 \\ \mu_x^{-1} \hat{k}_z^2 E_y + \mu_z^{-1} \hat{k}_x^2 E_y \\ 0 \end{pmatrix}. \end{aligned}$$

We thus obtain the equation of dispersion under s polarization,

$$\varepsilon_y = \frac{\hat{k}_z(\theta)^2}{\mu_x} + \frac{\hat{k}_x(\theta)^2}{\mu_z}, \quad (11)$$

where $\hat{k}_x(\theta) = n_0 \sin \theta$ in Fig. 1.

Combining Eqs. (5) and (11), we obtain the next equation:

$$\frac{\varepsilon_y}{\mu_x} = \left(\frac{n_0 \cos \theta}{\mu_0} \frac{1 - r_s(\theta)}{1 + r_s(\theta)} \right)^2 + \frac{n_0^2 \sin^2 \theta}{\mu_x \mu_z}. \quad (12)$$

When one knows the value of complex reflectivity r_s by optical measurement or computation, Eq. (12) is equation for ε_y/μ_x and $\mu_x \mu_z$. Two different angles ($\theta_1 \neq \theta_2$) yield $\sin \theta_1 \neq \sin \theta_2$, and enable to evaluate ε_y/μ_x and $\mu_x \mu_z$ uniquely.

By permutating the configuration $(x, y, z) \rightarrow (y, z, x)$, we can figure ε_z/μ_y and $\mu_y \mu_x$. Then, incident light sheds on the yz plane and has the polarization of $\mathbf{E}_{\text{in}} \parallel z$. The plane of incidence is the xy plane. In this second step, Eq. (12) is modified as

$$\frac{\varepsilon_z}{\mu_y} = \left(\frac{n_0 \cos \phi}{\mu_0} \frac{1 - \tilde{r}_s(\phi)}{1 + \tilde{r}_s(\phi)} \right)^2 + \frac{n_0^2 \sin^2 \phi}{\mu_y \mu_x}, \quad (13)$$

where \tilde{r}_s is complex reflectivity on the yx plane and ϕ is incident angle in the xy plane. In evaluating ε_z/μ_y and $\mu_y \mu_x$ similarly to ε_y/μ_x and $\mu_x \mu_z$, it is required that the object should be semi-infinitely thick along the x axis.

Since the relations of $\mu_x = \mu_y$ are assumed for SMDM, μ_x^2 is evaluated in the second step; succeedingly, the rest components of ε_x , ε_z , and μ_z are uniquely obtained except for the sign. The sign of μ_x is set to be $\mu_x \approx 1$ at 800 nm because the μ_x spectrum keeps constant and does not show any resonant behavior around the wavelength. The sign of μ_x at different wavelength is taken to avoid discontinuous jump as shown in Fig. 2.

Complex reflectivity r_s was computed exactly, whereas \tilde{r}_s was evaluated quite precisely, that is, within a-few-percent numerical error. The numerical way to compute \tilde{r}_s was reported earlier [20]. The precision in the computation for complex reflectivities ensures that the full components of tensors are determined within a-few-percent numerical error.

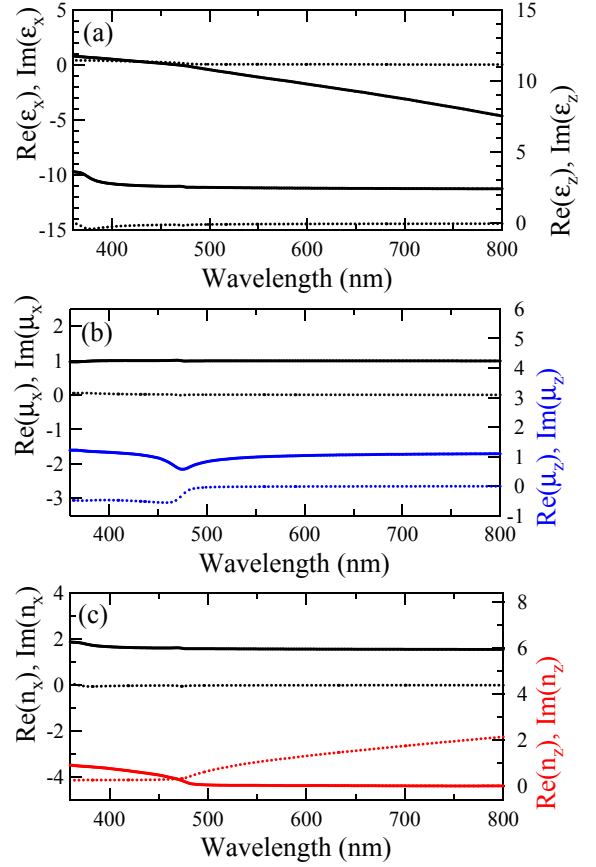


FIG. 2: Effective optical constants of SMDM, extracted with the two incident angles of 0° and 15° . The surface thickness d of SMDM is 20 nm. (a): Effective permittivity. Upper solid line denotes $\text{Re}(\varepsilon_x)$ and upper dotted line does $\text{Im}(\varepsilon_x)$. Lower two lines represent ε_z likewise. (b): Effective permeability. Lines indicate μ_x and μ_z with the notation similar to (a). (c): Effective refractive index along the x and z axes. The real parts are shown with solid lines and the imaginary parts with dotted lines.

III. NUMERICAL RESULTS

A. TCRM Analysis

Figure 2 presents the full components of (a) ε and (b) μ tensors of SMDM of surface thickness $d = 20$ nm. The tensors are extracted by TCRM with the two angles of 0° and 15° . Other sets of two incident angles result in the same spectra of ε_x , ε_z , and μ_x within the numerical error. This consistency indicates that ε_x , ε_z , and μ_x are independent of incident angle and consequently wavevector \mathbf{k} .

In TCRM analysis for SMDM using the angle pairs of $(0^\circ, \theta)$ and $(0^\circ, \phi)$, it is easily verified from Eq. (12) that μ_z depends only on the $\theta (\neq 0^\circ)$. The three components of ε_x , ε_z , and μ_x could in principal depend on the incident angles; however, they have been found to be independent of incident angles and therefore to be

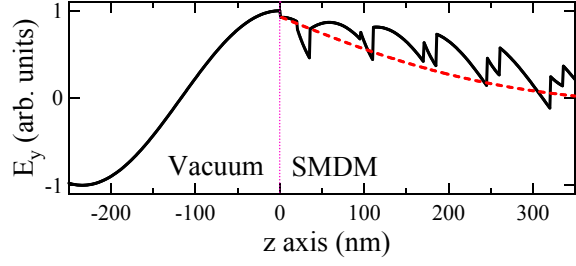


FIG. 3: Electric field vs the averaged field. Electric field is calculated at $\lambda_{p,\text{eff}}$ under normal incidence on the xy plane with s polarization. Solid line indicates forward propagation only, that is, incident and refractive components. Dashed line represents the electric field calculated by the effective refractive index n_z in Fig. 2(c). Vertical dotted line indicates the interface.

well-defined for SMDM. On the other hand, the component $\mu_z(\theta)$ is exceptionally evaluated for each non-zero θ . Thus, all the components of ε and μ tensors are determined self-consistently and in a well-defined manner at visible frequencies in Fig. 2.

The ε_x component has typical dispersion of Drude metal (upper solid and dotted lines in Fig. 2(a): the real and imaginary parts of ε_x , respectively), and the effective plasma frequency $\omega_{p,\text{eff}}$, which is defined by $\text{Re}[\varepsilon_x(\omega_{p,\text{eff}})] = 0$, is located at $\lambda_{p,\text{eff}} = c/2\pi\omega_{p,\text{eff}} = 468$ nm. On the other hand, the ε_z spectrum exhibits typical dielectric properties for the incident light of $\mathbf{E}_{\text{in}}||z$ on the xz or yz planes (lower solid and dotted lines in Fig. 2(a): the real and imaginary parts of ε_z , respectively). Concerning permeability components, μ_x is close to 1 at 360–800 nm (upper solid and dotted lines in Fig. 2(b): the real and imaginary parts of μ_x , respectively), while μ_z goes down to 0.57 at 477 nm and shows strong diamagnetism (lower solid and dotted lines in Fig. 2(b): the real and imaginary parts of μ_z , respectively). Refractive indexes along the x and z axes are displayed in Fig. 2(c); the upper solid and dotted lines respectively denote $\text{Re}(n_x)$ and $\text{Im}(n_x)$, and the lower solid and dotted lines respectively stand for $\text{Re}(n_z)$ and $\text{Im}(n_z)$. The imaginary parts of n_x and n_z are small below $\lambda_{p,\text{eff}}$, and correspond to efficient EM-wave propagation in SMDM.

In Fig. 3, we test the validity of description by effective refractive index at $\lambda_{p,\text{eff}}$. The interface of vacuum and SMDM is set at $z = 0$ and incident light illuminates on the xy plane normally. Solid line denotes electric field of incident light in vacuum ($z < 0$); it represents refractive component of electric field in SMDM ($z > 0$). Dashed line presents the effective field profile calculated by using n_z in Fig. 2(c) and reproduces the averaged field profile in SMDM approximately. Thus, TCRM extracts averaged EM response in SMDM. As was already confirmed in [20], the effective description has relevant physical meanings and works fairly well in the visible range of interest.

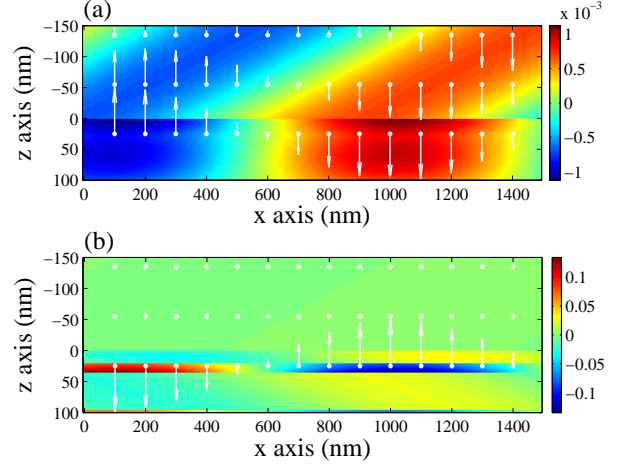


FIG. 4: Comparison of (a) B_z and (b) H_z at 477 nm, the minimum of $\text{Re}(\mu_z)$. The region of vacuum ($z < 0$) shows incident light only, for simplicity; the incident angle is $\theta = 15^\circ$. The region of SMDM ($z > 0$) contains both forwardly and backwardly propagating components. Arrows indicate the vectors at typical points (dots). In particular, the directions of B_z and H_z in metallic layer ($20 < z < 35$ nm) are clearly opposite.

B. Origin of effective diamagnetism

As shown in Fig. 2, effective diamagnetic response appears in the μ_z spectrum. This implies that magnetic induction B_z and magnetic field H_z behave in a different way. Figure 4 displays the actual distribution of (a) B_z and (b) H_z as image plot. Arrows denote the vectors at dotted points. The wavelength is at 477 nm, where $\text{Re}(\mu_z)$ is minimum. In vacuum ($z < 0$), the incident light travels with incident angle 15° ; only incident component is shown for simplicity in Fig. 4. In SMDM ($z > 0$), both forward and backward components are displayed simultaneously because reflectance R is not small ($R \sim 0.7$) and the backward components connected to inner multi-reflection is not negligible. The computation for B_z at each point is carried out from Eq. (6), and on the other hand magnetic field H_z is calculated from Eq. (7).

Figure 4 obviously shows that the directions of B_z and H_z are opposite in metallic layer ($20 < z < 35$ nm). Dielectric layers behave like paramagnetic materials. Besides, the H_z component in the metallic layer is far more intense than the H_z in vacuum and dielectric layers. In this way, the thin metallic layers are found to be diamagnetic along the z axis. The diamagnetic nature does not come from electronic spin states of silver but from the superimposed EM fields peculiar to mesoscopic structure of SMDM. The backward component is indeed responsible for the local diamagnetism. Thus, the effective diamagnetic μ_z response is found to originate from the thin metallic layers.

The diamagnetic response of metallic layer in SMDM

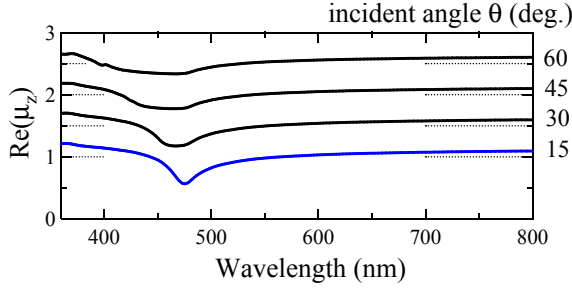


FIG. 5: Spatially dispersive behavior of μ_z resonance. All the spectra are obtained by TCRM with the two angles of 0° and $\theta (\neq 0^\circ)$. However, as described in the text, μ_z depends only on the θ in Fig. 1. The spectrum at 15° is the same with that in Fig. 2(b). The spectra at $\theta = 30^\circ, 45^\circ$, and 60° are offset for visibility by 0.5, 1.0, and 1.5, respectively. Horizontal dotted lines indicate $\text{Re}(\mu_z) = 1.0$ for each spectrum.

is confirmed numerically in Fig. 4. It is also easily derived from Maxwell equation. In Fig. 4, Eqs. (6) and (7) in a metallic layer are explicitly written as

$$i\omega B_z = ik_0 \hat{k}_x E_y, \quad (14)$$

$$\text{sgn}(\hat{k}_z) ik_0 \hat{k}_z H_x - ik_0 \hat{k}_x H_z = -i\omega \varepsilon_{\text{Ag}} E_y, \quad (15)$$

where $\text{sgn}(\hat{k}_z)$ takes 1 or -1 , and denotes the forward and backward propagation for the z axis. From the computation for actual EM distribution, $|H_z|$ is found hundreds times larger than $|H_x|$; *i.e.* $|H_z| \gg |H_x|$. Consequently, the first term in the left hand side of Eq. (15) is negligible to a good approximation. Then, deviding Eq. (14) by Eq. (15), the sign of the real part of B_z/H_z turns out to be determined by a factor ε_{Ag} :

$$\text{Re}(B_z/H_z) \propto \text{Re}(\varepsilon_{\text{Ag}}). \quad (16)$$

At the wavelength in Fig. 4, $\text{Re}(\varepsilon_{\text{Ag}}) < 0$ directly results in $\text{Re}(B_z/H_z) < 0$ in the metallic layer. Thus, the diamagnetic nature of thin metallic layers is confirmed from the simple calculation.

C. Properties of μ_z resonance

Figure 5 shows the dependence of μ_z on incident angle. The μ_z spectra in Fig. 5 vary for incident angles and indicates spatial dispersion. Note that μ_z at off-resonance above 540 nm is almost independent of θ . The spatial dispersion is a resonant behavior.

Figure 6 displays the effect of structure of unitcell on the effective μ_z . Figures 2–5 are the results regarding the surface thickness $d = 20$ nm; the spectra is shown again in Fig. 6. From bottom to top, the thickness d varies from 0 to 30 nm, respectively. By changing the surface thickness, the structure of unitcell in SMDM varies; see Fig. 1. SMDM with $d = 0$ and 10 nm show diamagnetic property in a wide range. The increase of surface thickness

d gradually reduces diamagnetism and finally eliminates the diamagnetism at $d = 30$ nm. Since the structure of unitcell directly affects the phase of EM wave in SMDM, it is crucially significant how to set the unitcell in realizing the effective diamagnetism. SMDMs of different unitcells are different metamaterials. Figure 6 is the explicit indication. It is also consistent with the conclusion in a recent numerical study [24], showing that the interfaces play a vital role in photonic slabs of finite thickness, in extracting effective constants by the retrieval way.

As is shown in Figs. 2 and 6, the effective diamagnetic response emerges at about $\lambda_{\text{p,eff}}$, comes from the stratified metallic layers in SMDM. In order to observe the diamagnetic resonance in SMDM, it is essential how to select the structure of unitcell. As the $\lambda_{\text{p,eff}}$ shifts with varying the ratio of metal in the unitcell, the diamagnetic resonance follows the shift of $\lambda_{\text{p,eff}}$. It strongly suggests that the diamagnetic resonance is magnetic part of the effective plasma resonance. The spatially dispersive behavior in Fig. 5 also shows a typical characteristic of resonance.

IV. DISCUSSION

From computational and theoretical studies, it was reported that effective magnetism takes place in the systems composed of dielectric [6, 25] and metallic rods [26, 27], results from the Mie resonances peculiar to the rods, and is spatially dispersive [6, 26]. These magnetic responses stem from the local resonance due to geometrical shape of constituents.

The effective diamagnetism in SMDM also inherited from the the local diamagnetic nature of thin metals, which was shown in Sec. IIIB. There is a remarkable characteristic to the diamagnetism of SMDM, which is absent in the systems of the local Mie resonance. In the Mie systems it is known that the resonances always induce not a small amount of absorption loss, whereas the diamagnetic resonance is almost free from loss as seen

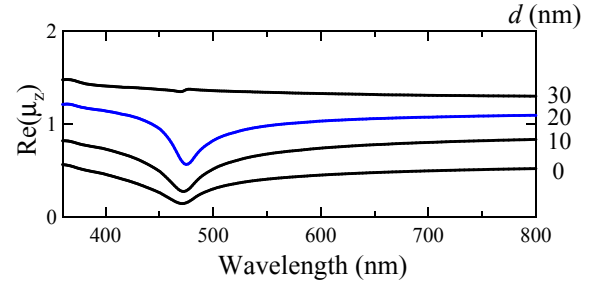


FIG. 6: Permeability μ_z spectra of SMDM with various unitcells: the thickness d of surface layers from 0 to 30 nm. All the spectra are computed at the incident angle of 15° , and are presented without vertical offset. The spectrum of $d = 20$ nm in Fig. 5 is displayed again for comparison.

in Fig. 2(c). Although small loss [*i.e.* small $\text{Im}(n_z)$] exists, it appears irrespective of the diamagnetism; indeed, the small loss also exists in the non-magnetic SMDM of surface thickness $d = 30$ nm in Fig. 6 [20]. This kind of magnetic resonance with low loss has not been found so far to our knowledge and is a new class of magnetism in metamaterials. Consequently, it is expected that low-loss, effective magnetic resonance at visible frequencies will be realized based on this magnetism.

Thick enough SMDM have been focused on in this paper. Of course, this system is not easily fabricated in reality. However, it is a good touchstone to examine how the effective optical responses emerge in periodic metal-dielectric systems. In the present analysis, there is no evidence to suggest negative refraction in SMDM, which was lately argued in finite systems [18, 19]. If negative refraction takes place in finitely thick SMDM, it would be due to an interference effect in finite systems.

V. CONCLUSIONS

The full components of effective tensors of ε and μ in SMDM has been numerically extracted by TCRM in a

well-defined way. As a main result, the effective strong diamagnetic resonance along the optical axis has been clarified. The resonance is spatially dispersive. It has been revealed that stratified thin metals in SMDM are the source of effective diamagnetism. The diamagnetism of thin metals results not from local Mie resonances but from the EM states realized in SMDM. The diamagnetic resonance is induced always near the effective plasma frequency; it can therefore be regarded as a magnetic component of the collective excitation. The diamagnetic nature of thin metals is experimentally feasible, and it will be a good test to measure nonlinear optical responses via diamagnetic resonance.

Acknowledgments

The author thanks T. Ishihara and S. G. Tikhodeev for stimulating discussion. This study was partially supported by Research Foundation for Opto-Science and Technology and by the Information Synergy Center, Tohoku University in numerical implementation.

-
- [1] J. B. Pendry and D. R. Smith, "Reversing Light With Negative Refraction," *Phys. Today* **57**(6), 37–43 (2004).
 - [2] V. M. Shalaev, "Optical negative-index metamaterials," *Nature Photon.* **1**, 41–48 (2007).
 - [3] D. R. Smith, S. Schultz, P. Markoš, and C. M. Soukoulis, "Determination of effective permittivity and permeability of metamaterials from reflection and transmission coefficients," *Phys. Rev. B* **65**, 195401 (2002).
 - [4] W. Lamb, D. M. Wood, and N. W. Ashcroft, "Long-wavelength electromagnetic propagation in heterogeneous media," *Phys. Rev. B* **21**, 2248–2266 (1980), and earlier references cited therein.
 - [5] D. J. Bergman, "Exactly Solvable Microscopic Geometries and Rigorous Bounds for the Complex Dielectric Constant of a Two-Component Composite Material," *Phys. Rev. Lett.* **44**, 1285–1287 (1980).
 - [6] D. Felbacq and G. Bouchitté, "Theory of Mesoscopic Magnetism in Photonic Crystals," *Phys. Rev. Lett.* **94**, 183902 (2005), and earlier references cited therein.
 - [7] J. C. M. Garnet, "Couleurs in Metal Glasses and in Metallic Films," *Philos. Trans. R. Soc. London* **203**, 385–420 (1904).
 - [8] J. C. M. Garnet, "Couleurs in Metallic Glasses, in Metallic Films, and in Metallic Solutions," *Philos. Trans. R. Soc. London* **205**, 237–288 (1906).
 - [9] D. R. Smith, D. C. Vier, T. Koschny, and C. M. Soukoulis, "Electromagnetic parameter retrieval from inhomogeneous metamaterials," *Phys. Rev. E* **71**, 036617 (2005), and earlier references cited therein.
 - [10] S. Zhang, W. Fan, N. C. Panoiu, K. J. Malloy, R. M. Osgood, and S. R. J. Brueck, "Experimental Demonstration of Near-Infrared Negative-Index Metamaterials," *Phys. Rev. Lett.* **95**, 137404 (2005).
 - [11] V. M. Shalaev, W. Cai, U. K. Chettiar, H.-K. Yuan, A. K. Sarychev, V. P. Drachev, and A. V. Kildishev, "Negative index of refraction in optical metamaterials," *Opt. Lett.* **30**, 3356–3358 (2005).
 - [12] G. Dolling, C. Enkrich, M. Wegener, C. M. Soukoulis, and S. Linden, "Low-loss negative-index metamaterial at telecommunication wavelengths," *Opt. Lett.* **31**, 1800–1802 (2006).
 - [13] L. D. Landau, E. M. Lifshitz, and L. P. Pitaevskii, *Electrodynamics of Continuous Media*, 2nd ed. (Pergamon, 1984).
 - [14] J. B. Pendry, "Negative Refraction Makes a Perfect Lens," *Phys. Rev. Lett.* **85**, 3966–3969 (2000).
 - [15] N. Fang, H. Lee, C. Sun, and X. Zhang, "Sub-Diffraction-limited Optical Imaging with a Silver Superlens," *Science* **308**, 534–537 (2005).
 - [16] M. Scalora, M. J. Bloemer, A. S. Manka, S. D. Pethel, J. P. Dowling, and C. M. Bowden, "Transparent, metallo-dielectric, one-dimensional, photonic band-gap structures," *J. Appl. Phys.* **83**, 2377–2383 (1998).
 - [17] L. Zhou, W. Wen, C. T. Chan, and P. Sheng, "Electromagnetic-Wave Tunneling Through Negative-Permittivity Media with High Magnetic Fields," *Phys. Rev. Lett.* **94**, 243905 (2005).
 - [18] M. Scalora, G. D'Aguanno, N. Mattiucci, M. J. Bloemer, D. de Ceglia, M. Centini, C. Sibilia, N. Akozbek, M. G. Cappeddu, M. Fowler, and J. W. Haus, "Negative refraction and sub-wavelength focusing in the visible range using transparent metallodielectric stacks," *Opt. Express* **15**, 508–523 (2007).
 - [19] J. Zhang, H. Jiang, B. Gralak, S. Enoch, G. Tayeb, and M. Lequime, "Toward -1 effective index with one-dimensional metal-dielectric metamaterial: a quantita-

- tive analysis of the role of absorption losses,” *Opt. Express* **15**, 7720–7729 (2007).
- [20] M. Iwanaga, “Effective optical constants in stratified metal-dielectric metamaterial,” *Opt. Lett.* **32**, 1314–1316 (2007).
- [21] P. B. Johnson and R. W. Christy, “Optical Constants of the Noble Metals,” *Phys. Rev. B* **6**, 4370–4379 (1972).
- [22] J. D. Jackson, *Classical Electrodynamics*, 3rd ed. (Wiley, 1999).
- [23] M. Born and E. Wolf, *Principles of Optics*, 7th ed. (Cambridge University Press, 1999).
- [24] T. Decoopman, G. Tayeb, S. Enoch, D. Maystre, and B. Gralak, “Photonic Crystal Lens: From Negative Refraction and Negative Index to Negative Permittivity and Permeability,” *Phys. Rev. Lett.* **97**, 073905 (2006).
- [25] K. C. Huang, M. L. Povinelli, and J. D. Joannopoulos, “Negative effective permeability in polaritonic photonic crystals,” *Appl. Phys. Lett.* **85**, 543–545 (2004).
- [26] D. Felbacq and G. Bouchitté, “Left-handed media and homogenization of photonic crystals,” *Opt. Lett.* **30**, 1189–1191 (2005).
- [27] X. Hu, C. T. Chan, J. Zi, M. Li, and K. M. Ho, “Diamagnetic Response of Metallic Photonic Crystals at Infrared and Visible Frequencies,” *Phys. Rev. Lett.* **96**, 223901 (2006).